Robot-assisted Tactile Sensing for Minimally Invasive Tumor Localization

A. L. Trejos
J. Jayender
M. T. Perri

Canadian Surgical Technologies and Advanced Robotics (CSTAR),
339 Windermere Road, London, Ontario, Canada
analuisa.trejos@lhsc.on.ca
jayender@gmail.com
mperri@uwo.ca

M. D. Naish

Department of Mechanical & Materials Engineering and Department of Electrical and Computer Engineering, The University of Western Ontario, and CSTAR,
London, Ontario, Canada
naish@eng.uwo.ca

R. V. Patel

Department of Electrical & Computer Engineering, and Department of Surgery,
The University of Western Ontario, and CSTAR,
London, Ontario, Canada
rajni.patel@lhsc.on.ca

R. A. Malthaner

Department of Surgery, The University of Western Ontario,
and CSTAR,
London, Ontario, Canada
richard.malthaner@lhsc.on.ca

Abstract

The 10 mm incisions used in minimally invasive cancer surgery prevent the direct palpation of internal organs, making intraoperative tumor localization difficult. A tactile sensing instrument (TSI), which uses a commercially available sensor to measure distributed pressure profiles along the contacting surface, has been developed to facilitate remote tissue palpation. The objective of this research is to assess the feasibility of using the TSI under robotic control to reliably locate underlying tumors while reducing collateral tissue trauma. The performance of humans and a robot using the TSI to locate tumor phantoms embedded into ex vivo bovine livers is compared. An augmented hybrid impedance control scheme has been implemented on a Mitsubishi PA10-7C to perform the force/position control used in the trials. The results show that using the TSI under robotic control realizes an average 35% decrease in the maximum forces applied and a 50% increase in tumor detection accuracy when compared to manual manipulation of the same instrument. This demonstrates that the detection of tumors using tactile sensing is highly dependent on how consistently the forces on the tactile sensing area are applied, and that robotic assistance can be of great benefit when trying to localize tumors in minimally invasive surgery.

KEY WORDS—minimally invasive surgery and therapy, smart instruments, tactile sensing, tumor localization, medical robotics

1. Introduction

Cancer is the second leading cause of death in North America and Europe. Worldwide, one in eight deaths is due to cancer, and, more particularly in the USA and Canada, cancer accounts for one in every four deaths (American Cancer Society

The International Journal of Robotics Research
Vol. 28, No. 9, September 2009, pp. 1118–1133
DOI: 10.1177/0278364909101136

Figures 1, 2, 4, 6–9, 11 appear in color online: http://ijr.sagepub.com

2007a, b). The best way to control the spread of cancer cells to healthy tissue or to other parts of the body is by surgically removing all of the cancer nodules through a procedure called surgical resection. Imaging techniques such as magnetic resonance imaging (MRI) or computed tomography (CT) scanning are critical for identifying the presence of lesions preoperatively. Intraoperatively, the surgeon relies on direct palpation of the tissue to confirm the tumor location or to find others that were not detected through imaging. Direct palpation of tissue provides a qualitative assessment of the mechanical properties of the tissue, since malignant tumors are commonly stiffer than the surrounding tissue, allowing them to be easily identified as hard nodules when palpated (Dargahi 2004).

Traditional tumor resection surgery involves performing a large incision in the chest or abdomen wall in order to access the diseased tissue, leading to a highly invasive procedure. The recent development of novel instruments and techniques has allowed surgical procedures to be performed through 10 mm incisions using long, narrow instruments. These minimally invasive approaches offer the advantages of reduced tissue trauma, decreased risk of infection, faster recovery time and reduced associated costs.

During surgery, the position of a tumor is often different from that in a preoperative scan due to tissue shift and, in the case of lung cancer surgery, collapsing of the lung. In minimally invasive surgery (MIS), the conditions for identifying tumor location are worsened by increased tissue shift due to insufflation of the abdomen or chest and the inability to directly palpate the tissue due to the size of the incision. Instead, standard MIS instruments are employed to probe the surface of the diseased organ, using any visual or tactile cues to determine the position of the tumor. The surgeon's ability to use these instruments for force feedback is compromised by the friction and moments introduced by the trocar and the cavity wall, and by the length of the instrument and the fulcrum effect at the incision site.

Laparoscopic ultrasound is an alternative method that is not dependent on kinesthetic feedback and is commonly used for tumor identification. However, this mode of imaging is not always available and its application to the lung is limited due to artifacts caused by residual air. In view of these limitations, an alternative method for locating tumors intraoperatively is required to improve the likelihood that a tumor resection can be completed using minimally invasive techniques, thereby providing all of the associated benefits.

One such method, which has been the subject of considerable research, is the relay of haptic cues, or the "sense of touch," from the tissue–instrument interaction to the surgeon–instrument interface. Haptic information can be considered in two distinct modes: kinesthetic and tactile (Ottermo et al. 2006). Kinesthetic information relates to the movement and bulk forces acting in the joints of an arm (human or mechanical) and at the point of contact. Such information may be used to assess the contour and stiffness of an object and may be acquired using a simple force/torque sensor. In contrast, tactile information includes the sensation of surface textures, or distributed pressures acting across the contacting surface. The measurement of tactile information requires a tightly packed array of sensors capable of measuring multiple contact pressures or forces concurrently. For a complete representation of tool–tissue interaction, information related to both the kinesthetic and tactile modes must be acquired.

1.1. Passive Measurement

A variety of instruments have been developed to measure tissue interaction forces when used in a handheld manner. These instruments are dependent on the user for proper operation – the instruments cannot position themselves or control the amount of contact force used during sensing.

A strain gauge sensorized laparoscopic grasper was developed by Bicchi et al. (1996). The grasping force and grasper position are presented along with a measure of compliance, which could be used to differentiate between objects of various stiffnesses. Another instrumented grasper, utilizing two thin foil strain gauges, is described by Dargahi (2004). This system is capable of operating in a wet saline environment due to silicone encapsulation of the electronics, and can determine the location of the applied force along the grasper jaws. The sensitivity can be adjusted by varying the amplifier gain, and the system was reported to be sensitive to a force increase of "a few grams." It was also shown through finite element analysis that the system could be used to measure distributed forces, approximating them as a concentrated load. A two-dimensional mechanical sensor to measure thrust and pull inside instrument jaws was proposed by Van Meer et al. (2004). The design of a laparoscopic grasper proposed by Tholey et al. (2004) uses piezoelectric sensors to detect forces in three degrees of freedom; however, the instrument is quite large for minimally invasive applications. In Singh et al. (2003), finite element analysis is used to evaluate the performance of a tooth-like sensor. Miniaturization of this device is still required. Rosen and Hannaford (2001) developed a sensorized grasper incorporating a six-degree of freedom (DOF) mini sensor (ATI Industrial Automation) and another force sensor on the grasper handle. Other researchers, such as Dubois (2002) and Shimachi et al. (2004), have also tried sensing the forces on the handle of the instrument. Bicchi et al. (1996) modified minimally invasive surgical tools by adding two strain gauges onto a sensing module and are used to estimate the properties of the manipulated tissue. Berkelman et al. (2003) proposed the use of a novel high-accuracy three-DOF miniature force sensor, 12.5 mm in diameter and 15 mm long, to internally measure tip forces by sensing forces on the shaft of the instrument.

A number of researchers have developed hand-held instruments that incorporate sensors directly onto the instrument gripper. A laparoscopic tactile sensor with a piezoelectric film

was proposed by Dargahi et al. (1999). Similarly, Takashima et al. (2005) proposed a tactile sensor that uses image processing to measure the relative motion between a transparent window and the end of an endoscope. An instrumented grasper was used to locate artificial tumors implanted in a porcine bowel by Schostek et al. (2006). While effective, it was found to be significantly slower than both direct palpation and the use of a standard instrument. Tactile feedback systems have also been proposed for the identification and characterization of lesions in the breast (Wellman and Howe 1997, 1999) and for identifying arteries during robotic surgery (Beasley and Howe 2002). The use of tactile sensors to identify pulmonary lesions using a capacitive array was discussed by Miller et al. (2007). Validation tests using a foam model showed promising results. A review of tactile sensing technologies suitable for MIS was presented by Eltaib and Hewit (2003).

1.2. Active and Robotic Measurement

Some of the difficulties encountered during MIS, due to the reduced access conditions, have been solved by the use of robotic systems. In these master–slave systems, the surgeon remotely and intuitively controls the instruments using the master controls, while a slave robot mimics the surgeon's motions and performs the procedure. The reversal of hand motion, force magnification, and poor dexterity are eliminated, while hand tremors are filtered and the view of the surgical field is magnified. One of the major limitations still present in MIS is the inability to transfer tool–tissue or hand–tissue interaction forces from the instrument tip to the surgeon.

A number of master–slave systems, capable of providing haptic feedback and suitable for the evaluation of tissue stiffness through palpation, have been developed. A computerized endoscopic surgical Babcock grasper that utilizes existing surgical tools was described by Hannaford et al. (1998) and Rosen et al. (1999). It performs an automatic palpation consisting of three cycles of a 1 Hz sinusoidal displacement of the grasper. Experimental results, indicating the tool's ability to distinguish different mechanical properties of tissues, appear promising. Tavakoli et al. (2005) measured tissue interaction using a number of strain gauges and a single-axis load cell integrated into a custom endoscopic instrument. User performance during soft tissue discrimination and lump localization was explored by Tavakoli et al. (2006a, 2006b). A different approach was used by Tholey et al. (2005), in which tissue stiffness was determined by measuring the amount of current applied to the motor of a motorized grasper.

The system developed by Dario and Bergamasco (1988) employs a robot to automatically palpate for a patient's arterial pulse at the wrist. The robot is instrumented with an anthropomorphic finger with a tactile sensor array in the fingertip. While not suitable for MIS procedures, this system stands out as the only previous automated system to use tactile sensing for diagnostic purposes.

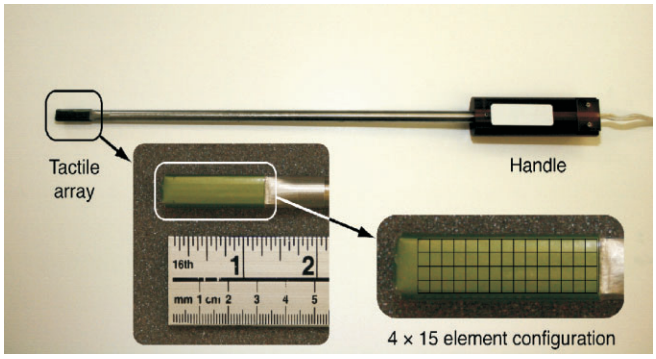

Fig. 1. TSI.

The research presented by Feller et al. (2004) evaluated the effect of using a master–slave robotic system equipped with tactile sensing capabilities to detect the presence of a 19 mm acrylic ball embedded in rubber. The results of using the robotic system were compared with the direct manipulation of the tactile sensor. Feedback to the user was provided via a tactile display. The results showed that the performance of the system was greatly dependent on how well the exploration force could be controlled by the user.

Some work in the area of robot-assisted palpation based on kinesthetic feedback has also been undertaken (McCreery et al. 2008). A slender probe was attached to a six-DOF force/torque sensor mounted on a PA10-7C manipulator. By advancing the probe to a constant depth from the surface of the tissue, the underlying tumors may be identified. This work also established the required measurement range and resolution for sensors used to perform palpation tasks.

1.3. Progress to Date

Based on the specifications determined by McCreery et al. (2008), a tactile sensing instrument (TSI) that uses a commercially available pressure pad was developed by the authors. The industrial TactArray sensor from Pressure Profile Systems (PPS) (Los Angeles, CA) was incorporated into a surgical probe suitable for MIS. Details of the sensor design can be found in Fearing (1990), Howe et al. (1995) and Peine et al. (1994). The TSI is shown in Figure 1. The PPS industrial TactArray on this instrument consists of an array with 15 rows and four columns of electrodes, which are oriented orthogonally to each other. Each overlapping area created by the row and column electrodes forms a distinct capacitor. Thus, the sensor used in this experiment contains a total of 60 distinct capacitors. A compressible dielectric matrix is used to separate the electrodes, which effectively acts as a spring between the electrodes. This capacitive array sensor technology is based on the phenomena that when pressure is applied on a capacitor, the decrease in distance between the two capacitor plates generates an increase in the output voltage. Once pressure is no

Table 1. Details of the TSI

Probe shaft length	385 mm
Probe shaft diameter	10 mm
Number of sensor elements	60
Area of each senor element	4 mm^2
Thickness of sensor	0.3 mm
Pressure range of sensor	0–14,000 kPa
Temperature range of sensor	–40°–200°C

longer applied to the sensor, the spring-like dielectric matrix allows the capacitor plates to return to their resting position. In order to address the biocompatibility issues of the probe, a disposable laparoscopic latex sleeve is placed over both the sensor and the shaft of the probe and can be replaced for each use of the probe. Details of the sensor and probe can be found in Table 1.

Other instruments have been developed for breast tumor localization using PPS sensors (http://www.pressureprofile.com). These instruments are not designed for MIS, which allows them to have a large sensing area, and as such, a large tissue area can be palpated at one time. In contrast, the instrument presented here is restricted to a 1 cm wide area so that it can be inserted through standard trocars. Preliminary tests showing the effectiveness of this hand-held probe, when compared to more traditional tumor localization methods, have been performed with promising results (Perri et al. 2008).

1.4. Objectives

The objective of this research is to assess the feasibility of using the TSI under robotic control in order to reduce tissue trauma and improve tumor detection. Furthermore, the research aims to develop an ideal robotic palpation method considering force and position control, the magnitude of the palpation force, the robot motion across the palpated tissue and a proper visualization technique. A section of this work has been presented by Trejos et al. (2008).

To achieve these objectives, an experimental evaluation has been performed. The experimental design is presented in Sections 2 and 3, starting with the details of the experimental setups used for the robot and the manual evaluations, and continuing with a thorough description of the experimental methods used. Section 4 summarizes the results obtained, which are then discussed in Section 5. A short conclusion is presented in Section 6.

2. Experimental Setup

Two experimental setups were used to compare the performance of a human and a robot when using tactile sensing for tumor localization. Both setups incorporated the use of the TSIs.

2.1. Manual Setup

The layout of the manual setup is shown in Figure 2. The TSI was used to palpate tissue resting on a plate that incorporates an ATI Gamma six-DOF force/torque sensor (Sensor A), (ATI Industrial Automation). To ensure consistency with minimally invasive procedures, the tray and the specimen were shielded by a drape during tissue palpation to ensure that the working field was not directly visible. A 0° scope with a standard resolution camera (Stryker Endoscopy, Inc) was held in place by the Aesop® endoscopic positioner.

The PPS driver and Sapphire® Visualization software were used to display the results from the tactile sensor in a meaningful way. This real-time pressure profiling system converts the measured voltage values from the capacitive sensor to pressure measurements, and displays these results in a color contour map of pressure distributions. The visualization software uses the visual color spectrum to indicate the levels of localized pressure intensity experienced by the probe, with pink indicating the highest pressure intensity and blue indicating the lowest pressure intensity. Therefore, a typical color contour map of a tumor would correspond to a region of a localized high pressure represented by pink (due to the stiffer nature of the tumor) surrounded by a region of low pressure indicated by blue (corresponding to softer tissue), thereby clearly distinguishing a tumor from the surrounding tissue. A grayscale version of this contour map is shown in Figure 3.

For the purposes of this experiment, an interpolated two-dimensional (2D) display of the visualization software was utilized since this display was found to be the most intuitive to interpret when using the probe for tumor localization. When insufficient forces are applied on the pad, or the sensitivity of the display is high, artifacts in the image make it difficult to distinguish the tumor location. A special feature in the software allows the user to set the sensitivity of the color contour pressure map for the active display window.

2.2. Robotic Setup

A seven-DOF Mitsubishi PA10-7C robot was employed to perform robot-assisted force-controlled tissue palpation. In our laboratory, the robot is controlled by a host computer via the ARCNET protocol. The four-layer control architecture consists of the host control computer, a motion control card, a servo controller and the robotic arm. The host computer communicates with the PA10-7C arm at a sampling rate of 333 Hz. The complete system used to perform the experiments is shown in Figure 4. The host computer (Intel Xeon 3.2 GHz, 3.48 GB RAM running Windows XP) controls the robot and sends data packets via the ARCNET protocol to the servo controller. The ARCNET card (PCI-20U from Contemporary Controls Inc.) has been modified to be compatible with the Optical Conversion Board (OCB) provided by Mitsubishi

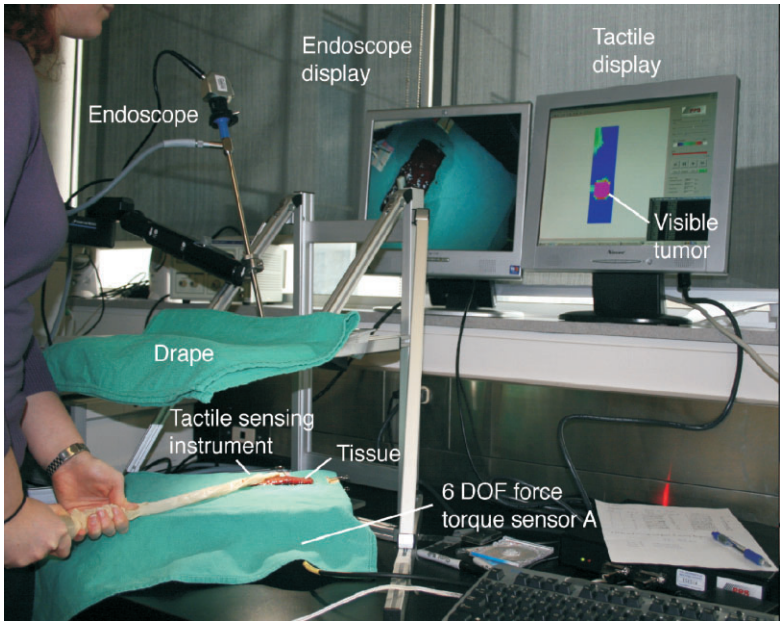

Fig. 2. Layout of the experimental setup for manual testing. The visualization software indicates the presence of a tumor.

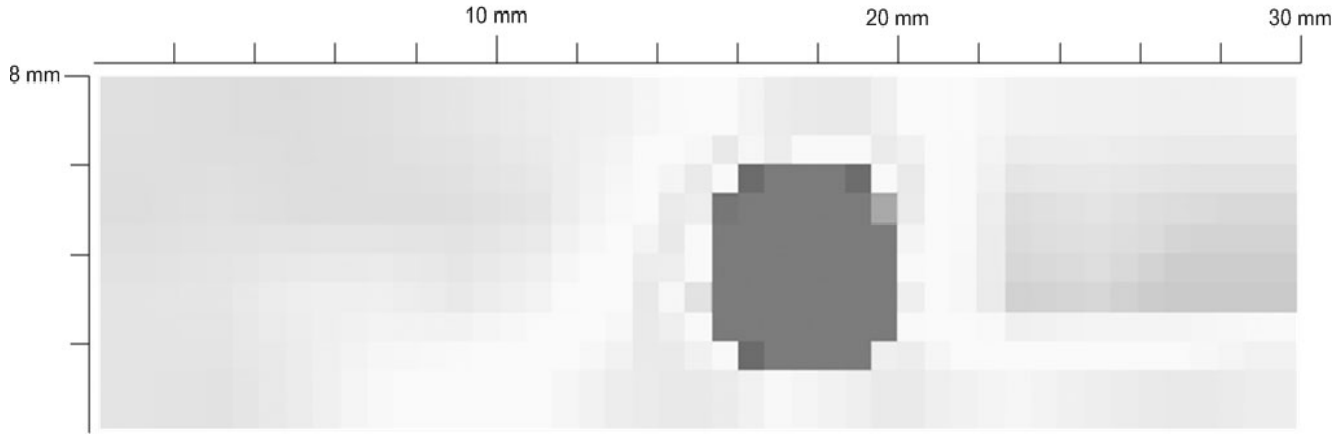

Fig. 3. A typical contour map of a tumor obtained from the visualization software.

Heavy Industries for the PA10-7C. An ATI Gamma six-DOF force/torque sensor (Sensor B) is used as the wrist force sensor on the robot to measure the force exerted by the robot end-effector on the tissue, assuming the instrument to be rigid. A second computer (Pentium IV 2.8 GHz, 1 GB RAM running Windows 2000 Professional) is responsible for data logging and visualization of the data obtained from the TSI.

In order to perform force-controlled tissue palpation, the robot must have the ability to control the amount of force exerted on the tissue and must move precisely in Cartesian space to palpate a grid of points on the surface of the tissue.

2.2.1. Robot Control

An augmented hybrid impedance control (AHIC) scheme was implemented on the PA10-7C robot to control the force of the palpation and the position of the end-effector in Cartesian space. The task space in AHIC is divided such that force control is performed in the direction of the palpation (in our case the z direction), while the position and orientation of the end-effector in the orthogonal directions are controlled. The area of the tissue palpated is based on the input provided by the user; however, palpation occurs in a completely autonomous manner.

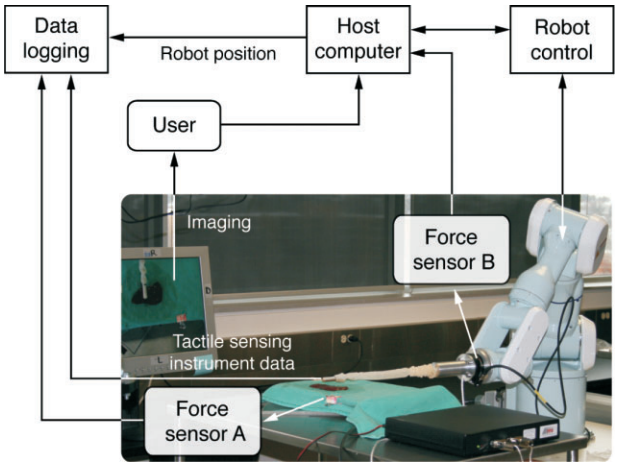

Fig. 4. Configuration of the robotic experimental setup.

In the AHIC scheme (Patel et al. 2008) there are two control loops. The outer loop takes the desired position and force profiles as input and generates the desired Cartesian acceleration that is fed to the inner loop. In the inner loop, the desired Cartesian acceleration is converted to joint acceleration. The desired torques for each of the links are then generated to track both the desired position and the force profiles. The block diagram is given in Figure 5. The AHIC algorithm consists of the modules outlined in Sections 2.2.2 to 2.2.4.

2.2.2. AHIC Module

The AHIC module can be defined as follows.

$$\ddot{X}_t = M_d^{-1}(-F_e + (I - S)F_d - B_d(\dot{X}_t - S\dot{X}_d) - K_d S(X_t - X_d)) + S\ddot{X}_d, \quad (1)$$

where M_d, B_d and K_d are the desired mass, damping and stiffness parameters, I is the identity matrix, F_d is the desired force, F_e is the environment contact force, X_t, $\dot{X}_t$ and $\ddot{X}_t$ are the target position/orientation, velocity and acceleration, respectively and X_d, $\dot{X}_d$ and $\ddot{X}_d$ are the desired position/orientation, velocity and acceleration, respectively. It should be noted that the target position/orientation is obtained from the desired position/orientation by means of Equation (1). The robot end-effector position/orientation is controlled to follow the target position/orientation and not the desired position/orientation. This modification is done to provide robust stability even in the presence of uncertainties in the model parameters. The matrix S denotes the selection matrix that defines the force and position controlled subspaces. The constraints of the tissue palpation problem are reflected in the S matrix. The behavior of the system is modeled by means of a mass (M_d), a spring (K_d) and a damper (B_d). These parameters define the damping ratio and the frequency of the system. The controller then ensures that the robot end-effector follows the response of this mass–spring–damper system. It should be noted that the parameters M_d, B_d and K_d cannot be arbitrarily modified to ensure accurate tracking of the force/position trajectories. In order to ensure accurate tracking in the presence of model uncertainties, an additional proportional-derivative (PD) loop is included where the PD gains were chosen to be high enough to ensure good trajectory tracking, but without the excitation of higher frequencies. The PD loop is given by the following equation.

$$\ddot{X}_r = \ddot{X}_t + K_p(X_t - X) + K_v(\dot{X}_t - \dot{X}), \quad (2)$$

where $\ddot{X}_r$ is the reference acceleration, K_p and K_v are the proportional and derivative gains of the PD loop and X and $\dot{X}$ are the Cartesian position/orientation and velocity of the end-effector respectively.

2.2.3. Redundancy Resolution Module

The redundancy resolution module (based on "configuration control" (Seraji et al. 1993; Patel and Shadpey 2005)), in the inner loop of the AHIC, converts the Cartesian acceleration to a desired joint-level acceleration and is provided to the joint-based controller. Since the PA10-7C robot has seven DOFs, the Jacobian is not square. As a result, an additional task is included to fix the redundant joint, thereby making the Jacobian square. A damped least-squares solution at the acceleration level (Patel and Shadpey 2005) is implemented to damp out the joint velocities in the null-space of the Jacobian as given by the following equation.

$$\ddot{\theta}_d = \left[J_e^T W_e J_e^T + J_c^T W_c J_c^T + W_v\right]^{-1} \times \left[J_e^T W_e(\ddot{X}_t - \dot{J}_e\dot{\theta}) + J_c^T W_c(\ddot{Z}) - W_v\lambda\dot{\theta}\right]^{-1}, \quad (3)$$

where $\ddot{\theta}_d$ is the desired joint acceleration, $\dot{\theta}$ corresponds to the joint velocities, $\ddot{Z}$ is the acceleration corresponding to the secondary task, J_e and J_c are the Jacobian matrices corresponding to the primary and the secondary tasks, W_e and W_c are the corresponding weight matrices, W_v is the singularity robustness factor and λ is the velocity damping factor. The joint accelerations are integrated to obtain the desired joint velocities and angles and fed to the joint control module after canceling the gravity term.

2.2.4. Joint-Based Controller

Each of the seven joints is controlled to follow a certain desired trajectory. The dynamic model for a rigid-link manipulator is given by

$$\tau = M(\theta)\ddot{\theta} + V(\theta, \dot{\theta}) + G(\theta), \quad (4)$$

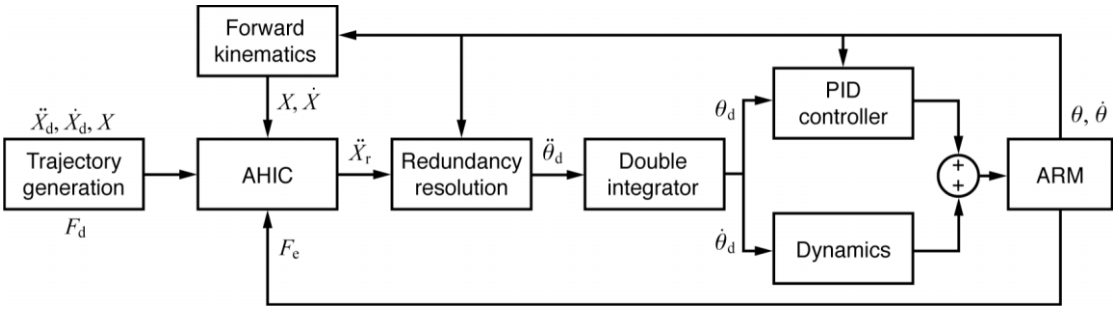

Figure 5. Flow diagram of the AHIC.

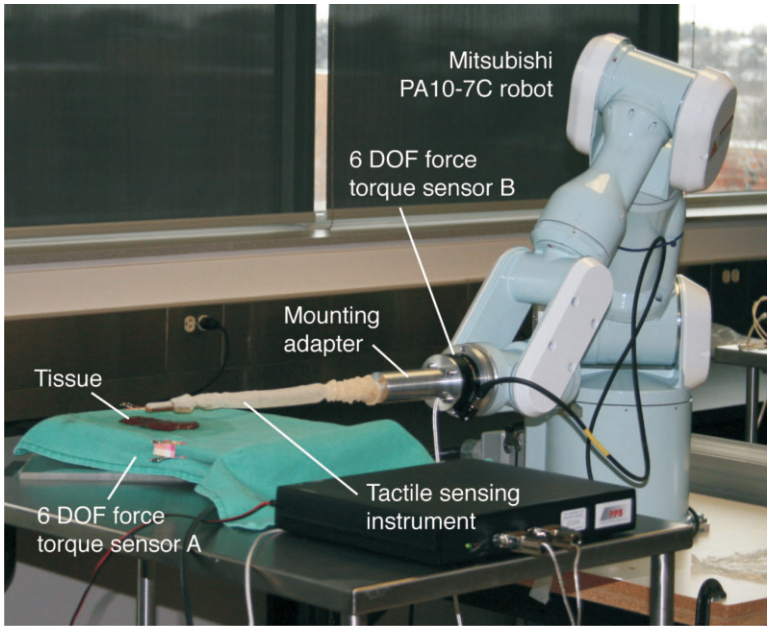

Fig. 6. Robotic setup palpating tissue.

where τ is the torque provided to each joint, $M(\theta)$ is the mass matrix, $V(\theta, \dot{\theta})$ is the vector of Coriolis and centrifugal terms and $G(\theta)$ is the vector of gravity terms. For medical robots, the joint velocities are generally quite small and this is also the case in this palpation application. Therefore, the $V(\theta, \dot{\theta})$ term can be assumed to be negligible. In addition, since there is very little change in the robot's configuration during palpation, the $M(\theta)$ term can be assumed to be constant. The gravity terms are obtained in closed-form. The joint level controller therefore simplifies to

$$\tau = \ddot{\theta}_d + K_{pj}(\theta_d - \theta) + K_{dj}(\dot{\theta}_d - \dot{\theta}) + G(\theta), \qquad (5)$$

where θ corresponds to the joint angles, θ_d and $\dot{\theta}_d$ are the desired joint angles and velocities, and K_{pj} and K_{dj} are the proportional and derivative gains of the joint level controller.

This control strategy was successfully implemented with the robotic setup shown in Figure 6. The experimental evaluation is explained in the following section.

3. Methods

An experimental evaluation was performed to compare the performance of the Mitsubishi PA10-7C robot to that of four human subjects when using tactile sensing for tumor localization. The details of this evaluation are presented below.

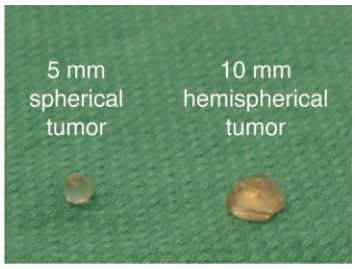

Fig. 7. Simulated tumors.

3.1. Tissue Preparation

The tissue used in these experiments was *ex vivo* bovine liver obtained from a local store. To simulate the presence of tumors, 5 mm diameter spherical objects and 10 mm diameter hemispherical objects (see Figure 7) were pressed into the dorsal side of the liver. These objects were made from thermoplastic adhesive (hot glue) with encased thin metal wires to ensure their visibility on radiographic images, which were later used to assess accuracy.

For each of the palpation methods, nine *ex vivo* livers were prepared with small tumors and nine with large tumors. Each sample had the possibility of containing from zero to two tumors, determined *a priori* through a block randomization process. Although in practice a patient will not be scheduled for surgery unless it is certain that a tumor is present in the organ, presenting liver with no embedded tumor allows the statistical results of specificity and negative predicted value to be determined. The block randomization process was designed to ensure that an equal number of cases of zero, one and two tumors embedded in the liver were presented at the end of all trials for each subject. The human subject was blinded to the block randomization, and allowed to practice using additional liver samples prior to commencing each series of trials.

3.2. Performance Assessment

The performance of each of the methods was assessed with different measurables: the success rate of locating tumors, the force exerted by the instrument while palpating and the task completion time.

The *success rate* of locating tumors aims to determine the ability of the sensing method to correctly identify all of the tumors present in each liver sample. The success rate can be determined using four categories (Davidson 2002): (1) a *true positive test* occurs when the tumor is correctly identified and found in the liver; (2) a *false positive test* occurs when the user indicates that a tumor is found where none is located in that area; (3) a *false negative test* occurs when the user did not find the tumor located in the liver; and (4) a *true negative test* occurs when the user correctly identifies that there is no tumor located in the liver. These four categories, adapted from Davidson (2002), can be used to determine measures such as accuracy (the proportion of tests that were correctly identified as having or not having a tumor), sensitivity (the proportion of tumors present in the samples that test positive), specificity (the proportion of specimens that do not have tumors and test negative), negative predictive value (the proportion of specimens that test negative that do not have tumors) and positive predictive value (the proportion of tumors found that are actually there, indicating the probability of a positive test of actually detecting a tumor).

The *palpation force* exerted while searching for a tumor is an indication of the potential damage to the tissue. In both setups, the maximum forces are determined using the ATI force/torque sensor placed below the specimen (Sensor A). The magnitude of the force vector is computed from the individual forces acting in all three orthogonal directions. For the manual trials, a continuous acquisition of the force data is recorded in Newtons (N) at a sample rate of 50 Hz. If there are any drag or frictional forces acting on the probe, these will be included in the measurements. For the robotic trials, the force values are recorded for each palpation point when the instrument is at its lowest position in contact with the tissue, i.e., when the applied force is at its maximum. The external forces acting on the probe (frictional, drag, viscous, etc.) have also been accounted for in the AHIC controller. The term F_e in Equation (1) corresponds to these forces.

Lastly, the *task completion time* is the time required to locate the tumors in the specimen presented during the task. The recorded time begins once the probe has touched the surface of the liver. The task completion time is recorded once the user stops palpating the tissue, signifying the end of the trial.

3.3. Manual Tests

Four human subjects participated in this experiment: two of them were experienced in surgical oncology and MIS; the other two had no medical background. To further reduce the error attributed to a learning curve, the human participants were permitted to practice palpating 5 mm and 10 mm diameter tumors embedded into the livers with the TSI until comfortable with its performance. These livers were prepared exclusively for the training sessions and were not selected for use during the trials.

Before the commencement of the trials, the participants were informed that any number of tumors could be located in the presented liver (including no tumors). A total of eighteen trials were completed by each of the four subjects to locate the artificial tumors (nine livers with 10 mm tumors and nine with 5 mm tumors). The livers used in each trial were randomly assigned to the subjects; however, it was ensured that the human subjects would each palpate the same number of tumors as the robot.

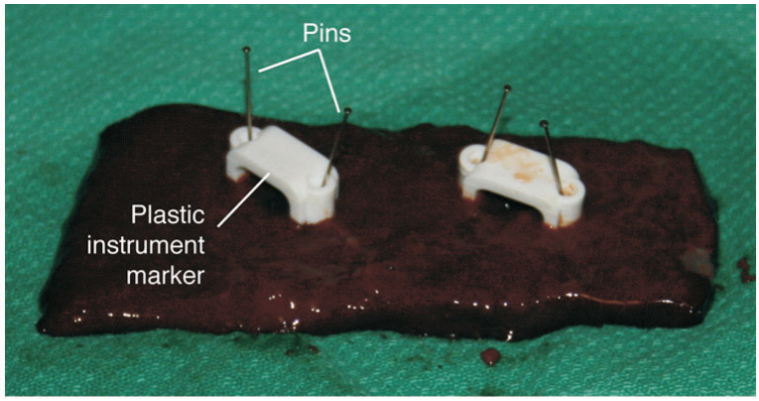

(a)

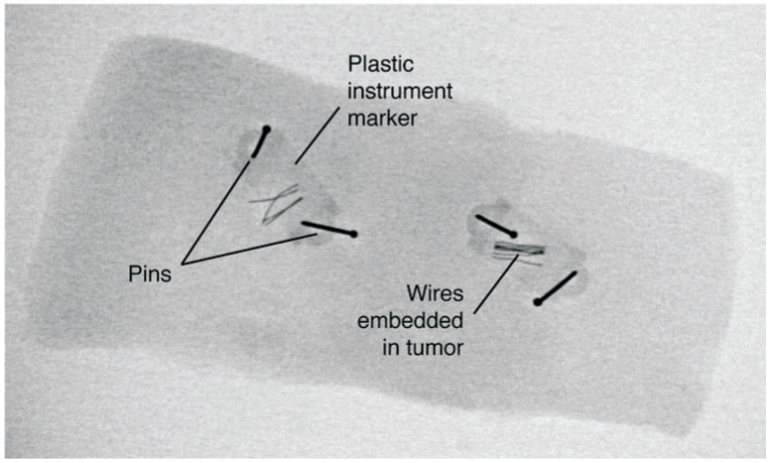

(b)

Fig. 8. (a) Manually palpated tissue with each suspected tumor site marked by a plastic instrument marker held in place with two pins. (b) Radiograph of tissue, 10 mm tumors with embedded wire and plastic instrument markers.

During the trials, the task completion time and the palpation force as indicated by Force Sensor A were recorded. The location of the tumors found by the participants were marked using a plastic instrument marker and two marking pins (Figure 8(a)). The recorded task completion time did not include the time taken to place each marker.

To assess the success rate of the tumor localization method, all livers were imaged using a fluoroscopic radiographic machine after palpation. Both the tumors and the plastic markers are clearly evident in these images (Figure 8(b)). As such, a true positive result is achieved when there is an evident intersection between the area of the tumor and the area of the plastic instrument marker in the radiographic image. It was decided that intersection rather than the entire encapsulation of the tumor with the instrument marker is sufficient to demonstrate proper localization. This mitigates any errors that may have been introduced during marker placement on the tissue. When a tumor was not correctly identified, a false negative result was recorded. A false positive result was recorded when a marker was noted in the radiograph image where there was no tumor present. A true negative test was recorded in cases in which the liver presented to the subject had no tumors and the subject correctly identified it as such.

3.4. Robotic Tests

The user interface for the robotic setup allowed the user to input the direction of palpation, and the number of points to palpate, while the robot autonomously palpated these points. Two different methods of robotic palpation were implemented: force control and position control.

In the force control setting, the robot approaches the tissue under force control (in the z direction) until the wrist force sensor (Sensor B) registers a desired force. Once the desired force has been reached, the robot end-effector coordinates, corresponding to the tissue surface coordinates, are transmitted to the client. Instantaneously, the readings from the TSI are

recorded to register the force profile of the contact made with the tissue. The robot is then commanded to move up (z direction) and sideways (x or y direction) in 3 mm steps through position control to the next point. This process continues until all of the desired points specified by the user have been palpated. In order to choose the desired force of palpation, preliminary tests were done with a 2 N palpation force; these tests showed a poor success rate caused by image artifacts in the contour map. Subsequent tests using a 4 N palpation force showed a significant improvement in preliminary results with no noticeable tissue damage. In a similar study performed by the authors, it was found that the average maximum force applied by surgeons when manually palpating *ex vivo* liver with 10 mm tumors was 4.4 N. Thus, a palpation force of 4 N was selected for the experimental evaluation.

In the position control setting, the user provides the same commands to the robot as in the force control setting. The difference between these settings lies in how deeply the instrument palpates the tissue. The position of the end-effector is controlled in all Cartesian directions ($S = I$). The desired trajectory in the z direction was generated such that the robot was commanded to make contact with the surface and move below the surface under position control. However, the readings from Sensor B were constantly polled to detect when contact was made with the tissue and to determine when the force of contact reached the 4 N threshold. The robot would then move upwards and continue to the next point until the entire area defined by the user was palpated.

For all tests performed by the PA10-7C robot, the palpated livers were assessed using a custom-designed software program that records the position of the robot and the force exerted on the tissue by the robot. During post-processing of the experimental data, a 3D graphical representation of position (x direction, y direction) versus palpation force of the robot was generated. The palpation force consists of the data gathered from the tactile sensor during the trial. The topographical (2D) view of this graph serves to indicate the tumors located by the robot, presented as a color map with pink indicating the highest forces and blue indicating the lowest forces exerted on the TSI. The analysis and assessment of the 2D plot was performed by four human volunteers who were blinded to the number of tumors present and the control method used in each trial. The purpose of having four subjects perform the assessment was to provide an unbiased record of the location and number of tumors that were located by the robot in each of the methods. To ensure that no bias towards either robot method was possible, the images presented to the volunteers were randomized and the file names altered. A similar assessment of the success rate was performed and compared to that of the human subjects.

The Statistical Package for Social Sciences (SPSS, Chicago, IL) software, version 15.0 for Windows, was used for the statistical analysis of the force and time measurements. A one-way analysis of variance (ANOVA) was performed to establish differences among the methods. Due to the samples having unequal variances, the Dunnett test was then performed to determine significant differences between the individual groups. Unpaired t-tests were used to determine differences between the large and the small tumors within each group.

4. Results

The experimental results from the force and position control methods were quite similar. The main difference was that the force control method showed marginally better performance for smaller tumors over the position control method. Therefore, only the detailed results from the force control method are shown in this paper. The results for position control are summarized in Tables 2 and 3 for comparison.

The results of force control on the PA10-7C, which are given in Figure 9(a)–(c), show the trajectory tracking of the end-effector in Cartesian space corresponding to the x, y and z coordinates. The selection matrix S in the AHIC scheme is chosen such that, while palpating the tissue, force control is performed in the z direction while position control is performed in the x and y directions ($S = \text{diag}\{1,1,0,1,1,1\}$). Consequently, Figure 9 (a) and (b) show accurate tracking of the position trajectory in the x and y directions by the robot end-effector. In Figure 9(c), it can be observed that the robot starts by palpating one point to establish the location of the tissue. The pauses observed in the robot motion correspond to when the robot is waiting for the user to enter the desired direction of palpation and the number of palpation points. This figure also shows that the robot approaches the tissue under force control and consequently does not follow the desired Cartesian trajectory. Once the force of palpation as recorded by Sensor B reaches the desired force (shown in Figure 9(d)), the robot is commanded to move to the next point under position control in all directions ($S = \text{diag}\{1,1,1,1,1,1\}$), as can be seen in Figure 9(a)–(c). The switching between force and position control is highlighted in the time interval from 22.6 seconds to 25.5 seconds in Figure 9(c).

Sample graphs showing grayscale versions of the pressure maps obtained when the robot palpated the tissue are presented in Figure 10. The results of the experimental evaluation are summarized in Tables 2 and 3. Table 2 shows the mean of the maximum force applied in the eighteen trials (nine trials with small tumors and nine with large tumors) with each of the methods, and the associated p-values. These results show that there is a significant difference in the forces applied by the human in comparison to the robotic methods, but that there is no significant difference between the forces applied within the robotic methods. It was also found that in the human trials, the application of forces greater than 6 N for extended periods of time caused visible damage to the tissue. An example of a tissue after human palpation, in which a maximum force of 10.6 N was applied, is shown in Figure 11. It should be noted that

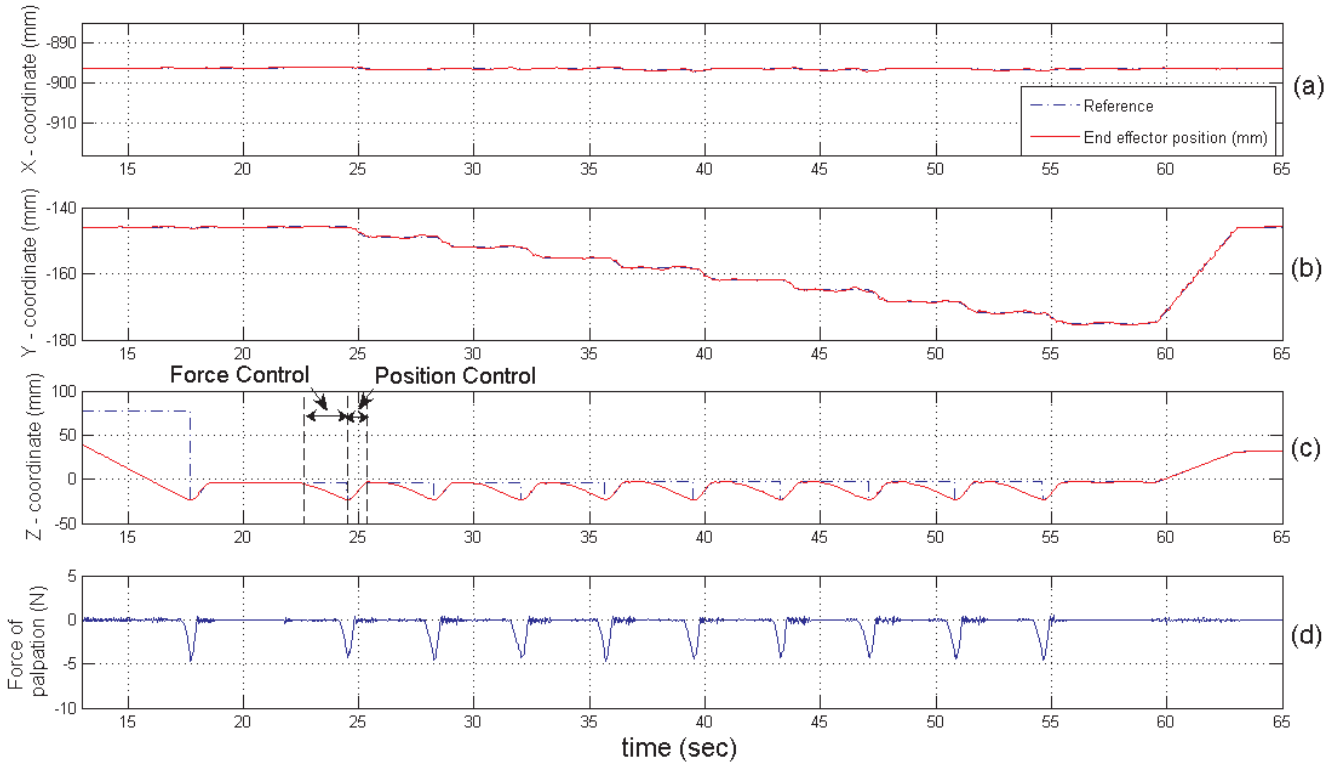

Fig. 9. Trajectory tracking of the robot end-effector under force control.

no studies have been found that provide a relationship between palpation forces and tissue damage. A study presented in De et al. (2007) provides a good evaluation of tissue damage caused by gripping. However, the pressures found to cause damage in their study (above 100 kPa) are much greater than the forces applied herein (a range of 6–11 N corresponds to 20–37 kPa), thus indicating that the methods do not provide an adequate basis for comparison.

Also shown in Table 2 is the average task completion time. The average times for the two robotic methods are significantly different; however, the task completion time for the human and robot trials cannot be compared directly. While the task completion time for the robot includes only the palpation time, the task completion time for the human also included the time it took to assess the information.

Table 3 shows the measures of accuracy typically used to assess the effectiveness of a diagnostic test. This analysis was performed as a way of assessing the effectiveness of the TSI to determine tumor presence, and shows a significant improvement in all of the measures when using robotic assistance to control the motion of the instrument. For the robot trials, the Fleiss' kappa was used to determine the degree of agreement among the assessors of the pressure maps. A score of 0.89 was obtained, placing the results in the "almost perfect agreement" range.

5. Discussion

The results of this study show that using a tactile sensing MIS instrument under robotic control reduces the maximum force applied to the tissue by more than 35% (from 8.13 to 5.24 N) compared to manual manipulation of the same instrument. Furthermore, detection accuracy is increased by more than 50% (from 59% to at least 90%, depending on the robot control method used for palpation).

The primary difference between robot and manual tissue palpation is that the robot can apply a consistent amount of force at each step and can move systematically over the entire surface of the tissue, thereby producing a complete, contiguous map of the entire surface. This is equivalent to having one tactile pad that covers the entire specimen and applying an ideal force to the entire surface of the tissue (similar to the tactile sensors that have been developed for breast tumor detection). When a human palpates tissue, he or she does not know how much force is being applied compared to how much force was applied on another area of the tissue. Therefore, a particular feature might be highlighted only because a higher palpation force is being applied in that area (or the contact angle between the instrument and the tissue becomes more oblique), or a tumor might not be detected only because a lower palpation force is being applied in that area. Although only the subjects with surgical experience have a basis for knowing how much

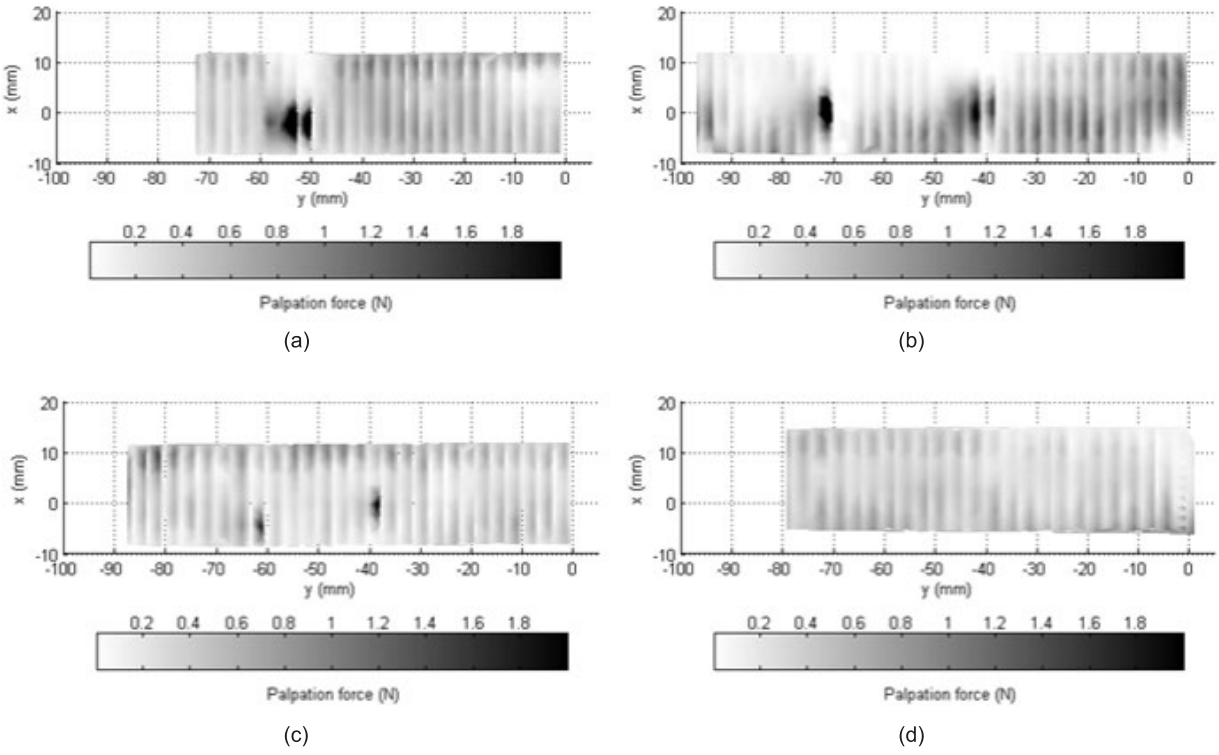

Fig. 10. Sample grayscale pressure maps for the robot palpation experiments: (a) one large tumor, (b) two large tumors, (c) two small tumors and (d) no tumors.

Table 2. Maximum Forces Applied and Task Completion Time for the Various Tests

	Maximum force (N)	*p*-values for force	Average time (s)	*p*-values for time
A – Human				
Small tumors	8.14 ± 2.9	0.970 small to large	217.5 ± 126.2	0.173 small to large
Large tumors	8.12 ± 3.6		176.8 ± 124.9	
Average	8.13 ± 3.2	<0.001 to B and C	197.2 ± 126.4	
B – Robot force control				
Small tumors	4.96 ± 0.1	0.180 small to large	129.8 ± 25.0	0.078 small to large
Large tumors	5.38 ± 0.9		156.0 ± 33.2	
Average	5.17 ± 0.63	<0.001 to A, 0.784 to C	142.9 ± 31.5	<0.001 to C
C – Robot position control				
Small tumors	5.10 ± 1.3	0.537 small to large	96.2 ± 16.7	0.224 small to large
Large tumors	5.38 ± 0.3		105.0 ± 12.3	
Average	5.24 ± 0.9	<0.001 to A, 0.784 to B	100.6 ± 14.9	<0.001 to B

pressure could cause damage, both surgeons and non-surgeons caused very similar tissue damage. It was found that if the subjects observed an increase in pressure on the visual display, the tendency was to focus on that area, applying increased forces to see if the feature observed was in fact a tumor. This led to the significant increase in the applied forces and in the task completion times. This highlights the advantage of using a robot, since humans require a great deal of experience to ensure

Table 3. Accuracy Measures of the TSI as a Diagnostic Instrument, with and without Robotic Assistance

Trial	Accuracy	Sensitivity	Specificity	Positive predictive value	Negative predictive value
Human					
Small tumors	49%	67%	22%	57%	29%
Large tumors	69%	94%	30%	68%	78%
Average	59%	81%	26%	63%	46%
Robot force control					
Small tumors	87%	92%	75%	89%	80%
Large tumors	98%	97%	100%	100%	92%
Average	92%	94%	86%	94%	86%
Robot position control					
Small tumors	83%	78%	100%	100%	60%
Large tumors	96%	94%	100%	100%	86%
Average	90%	86%	100%	100%	71%

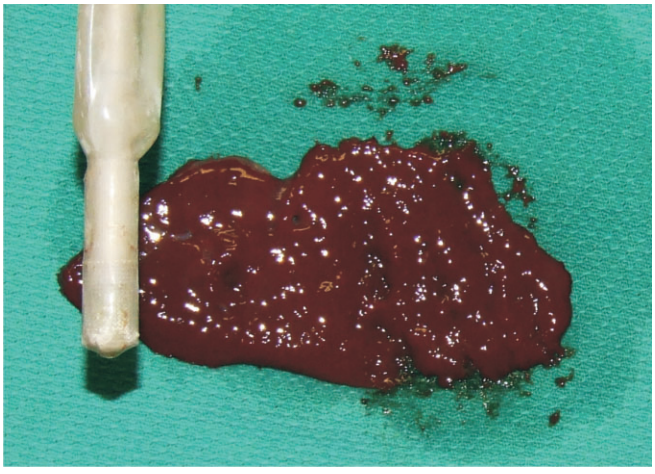

Fig. 11. Damaged tissue due to excessive force applied during manual palpation.

that excessive force is not being applied to the tissue. Even with experience, subjects cannot always control the amount of force being applied. The advantage of using a robot is that it can restrict the applied force to lie within safe limits.

As mentioned earlier, in order to meet the requirements of MIS, it was necessary to reduce the palpation area to 1 cm in width. In most cases, this area is not enough to fully capture an existing tumor. It is then necessary to compare adjacent pressure maps to identify if a tumor is present. When building a piecewise map, the benefit of applying a consistent palpation force is significant, allowing the narrow instrument to approximate the performance of larger devices designed for non-MIS applications.

When comparing the force and position control robot palpation methods, there is no clear method that performed better than the other. Both methods applied the same amount of force, while position control reduced task completion time by about 40%. However, force control provides better accuracy and sensitivity measures, which are the most significant indicators that a greater proportion of tumors have been correctly identified.

Preliminary tests performed with the robotic setup showed that the best palpation method was to start at one end of the tissue and move in 3 mm steps towards the other side of the tissue, taking measurements from a single pass over each area that may contain a tumor. Due to the way the data was plotted, if multiple directions of palpation were performed and there was a significant overlap between the areas palpated, the visualization software was less capable of detecting the presence of tumors. A force of 4 N was found to be the ideal force required to obtain consistent results when trying to locate 5 and 10 mm tumors; however, it should be noted that for different types of tissue and different tumor sizes, the optimal palpation force would be different.

As expected, all of the methods performed better when detecting 10 mm tumors than when detecting 5 mm tumors. It should be noted that, the "large" tumors used in this study are not clinically large. In fact, most diagnostic tests are not capable of detecting tumors that are smaller than 10 mm (LeBlanc et al. 2007; Singh et al. 2007). The smaller 5 mm tumors were included in this study to properly assess the improvement of one method over another under the worst-case scenario.

The measures of accuracy, sensitivity, specificity and negative and positive predictive values are those commonly used to quantify the effectiveness of diagnostic tests. These measures are based on the number of patients that are successfully or unsuccessfully identified as having or not having the disease in

question. In this study, the calculation of these measures was modified to include the number of tumors present, so that if a specimen contained two tumors, and only one was correctly identified, the measures of accuracy and sensitivity will reflect this outcome. Also, if a specimen contained only one tumor and an additional one was incorrectly found, the measure of specificity was also penalized.

It was determined that the most intuitive way of presenting the information obtained during the robotic experiments to identify tumor location was to plot the data on a 2D map representing the surface (superior view) of the liver, with the information from the tactile sensor overlaid directly on this map. This was accomplished by post-processing the data and assessing the resulting graphs. However, in a clinical setting, it would be ideal if this map were generated in real-time, so that if desired, the surgeon can repeatedly palpate an area of interest with a different force, a different step size, or using a different control method.

An instrument of this type would be especially beneficial for lung tumor resection in which tissue shift is significantly greater due to lung collapse, and where the effectiveness of laparoscopic ultrasound is compromised by air within the lung, making it very difficult to locate tumors that are less than 10 mm in diameter.

It should be noted that the presented system is not at a stage in which it can be used in a clinical setting. First of all, the robotic system used is an industrial robot that is not safe to operate in close proximity to humans. Furthermore, the motion of the instrument is not designed to mimic the remote center of motion required for MIS, where the instrument is inserted through a trocar in order to enter the patient's body. In order to properly palpate tissue through a trocar, the sensing instrument must be designed to have a flexible or articulating head to ensure that the sensing pad can be placed parallel to the tissue and obtain a proper pressure distribution on the sensor itself. Once the sensing pad can be properly oriented, it would be straightforward to adapt the TSI to currently available surgical robotic systems.

In our future work, a virtual remote center of motion will be incorporated into the robot controls in order to assess the ability of robotically locating a tumor when the instrument enters the surgical area through a trocar. The possibility of integrating the TSI into the ZEUS® Surgical System will also be considered. A TSI with an articulating head will be developed for this purpose.

An additional modification to the control schemes will include a user-selectable and/or adaptive palpation step size in order to increase the number of palpations around a suspicious area. For this purpose, a master–slave interface (that still ensures consistent palpation force and a systematic movement across the surface) will be implemented. The increased control achievable through a master interface could overcome the fear that surgeons may have about the use of robots in surgery. Furthermore, the feasibility and effectiveness of combining tactile and kinesthetic feedback for tumor localization will be determined.

6. Conclusions

The results of this study show that robotic assistance realizes a 55% decrease in the maximum forces applied on tissue, a 50% decrease in task completion time and a 40% increase in tumor detection accuracy. The use of robotic assistance for tactile sensing during MIS is not only feasible, but results in reduced tissue trauma and increased tumor detection compared to the manual manipulation of a TSI.

Acknowledgements

The authors would like to thank Greig McCreery for his work on the development of the TSI and Adam Katchky, Dave Bottoni and the CSTAR staff for their help and support with this work. This research was supported by the Natural Sciences and Engineering Research Council (NSERC) of Canada under grants RGPIN-1345 (R.V. Patel), and 312383 (M. D. Naish), by the Ontario Research and Development Challenge Fund under grant 00-May-0709; and by infrastructure grants from the Canada Foundation for Innovation awarded to the London Health Sciences Centre (Canadian Surgical Technologies & Advanced Robotics) and to The University of Western Ontario (R. V. Patel).

References

American Cancer Society (2007a). *Cancer Facts and Figures 2007*, No. 500807. Atlanta, GA, American Cancer Society Inc. http://www.cancer.org.

American Cancer Society (2007b). *Global Cancer Facts and Figures 2007*, No. 861807. Atlanta, GA, American Cancer Society Inc. http://www.cancer.org.

Beasley, R. A. and Howe, R. D. (2002). Tactile tracking of arteries in robotic surgery. *Proceedings of the IEEE International Conference on Robotics and Automation*, Vol. 4, Washington, DC, pp. 3801–3806.

Berkelman, P. J. et al. (2003). A miniature microsurgical instrument tip force sensor for enhanced force feedback during robot-assisted manipulation. *IEEE Transactions on Robotics and Automation*, **19**(5): 917–922.

Bicchi, A. et al. (1996). A sensor-based minimally invasive surgery tool for detecting tissue elastic properties. *Proceedings of the IEEE International Conference on Robotics and Automation*, Vol. 1, Minneapolis, MN, pp. 884–888.

Dargahi, J. (2004). An integrated force–position tactile sensor for improving diagnostic and therapeutic endoscopic

surgery. *Bio-Medical Materials and Engineering*, **14**(2): 151–166.

Dargahi, J., Payandeh, S. and Parameswaran, M. (1999). A micromachined piezoelectric teeth-like laparoscopic tactile sensor: theory, fabrication and experiments. *Proceedings of the IEEE International Conference on Robotics and Automation*, Detroit, MI, pp. 299–304.

Dario, P. and Bergamasco, M. (1988). An advanced robot system for automated diagnostic tasks through palpation. *IEEE Transactions on Biomedical Engineering*, **35**(2): 118–126.

Davidson, M. (2002). The interpretation of diagnostic tests: a primer for physiotherapists. *Australian Journal of Physiotherapy*, **48**: 227–232.

De, S. et al. (2007). Assessment of tissue damage due to mechanical stress. *The International Journal of Robotics Research*, **26**(11–12): 1159–1171.

Dubois, P. (2002). *In vivo* measurement of surgical gestures. *IEEE Transactions on Biomedical Engineering*, **49**(1): 49–54.

Eltaib, M. E. H. and Hewit, J. R. (2003). Tactile sensing technology for minimal access surgery – a review. *Mechatronics*, **13**: 1163–1177.

Fearing, R. S. (1990). Tactile sensing mechanisms. *The International Journal of Robotics Research*, **9**(3): 3–23.

Feller, R. L. et al. (2004). The effect of force feedback on remote palpation. *Proceedings of the IEEE International Conference on Robotics and Automation*, New Orleans, LA, pp. 782–788.

Hannaford, B. et al. (1998). Computerized endoscopic surgical grasper. *Proceedings of Medicine Meets Virtual Reality 6*, San Diego, CA, pp. 111–117.

Howe, R. D. et al. (1995). Remote palpation technology. *Engineering in Medicine and Biology Magazine*, **14**(3): 318–323.

LeBlanc, J. K., DeWitt, J. and Sherman, S. (2007). Endoscopic ultrasound: how does it aid the surgeon? *Advances in Surgery*, **41**: 17–50.

McCreery, G. L. et al. (2008). Feasibility of locating tumors in lung via kinesthetic feedback. *International Journal of Medical Robotics and Computer Assisted Surgery,* published online, DOI: 10.1002/rcs.169.

Miller, A. P. et al. (2007). Tactile imaging system for localizing lung nodules during video assisted thoracoscopic surgery. *Proceedings of the IEEE International Conference on Robotics and Automation,* Rome, Italy, pp. 2996–3001.

Ottermo, M. V. et al. (2006). The role of tactile feedback in laparoscopic surgery. *Surgical Laparoscopy Endoscopy and Percutaneous Techniques*, **16**(6): 390–400.

Patel, R. V. and Shadpey, F. (2005). Control of redundant robot manipulators: theory and experiments. *Lecture Notes in Control and Information Sciences*, Vol. 315. Heidelberg, Springer.

Patel, R. V. et al. (2008). A robust position and force control strategy for 7-DOF redundant manipulators. *IEEE Transactions on Mechatronics*, accepted.

Peine, W. J., Son, J. S. and Howe, R. D. (1994). A palpation system for artery localization in laparoscopic surgery. *Proceedings of the 1st International Symposium on Medical Robotics and Computer Assisted Surgery*, Pittsburgh, PA.

Perri, M. T. et al. (2008). A new tactile imaging device to aid with localizing lung tumours during thoracoscopic surgery. *Proceedings of the International Conference on Computer Assisted Radiology and Surgery (CARS)*, 22nd International Congress Series, Barcelona, Spain.

Rosen, J. and Hannaford, B. (2001). Markov modeling of minimally invasive surgery based on tool/tissue interaction and force/torque signatures for evaluating surgical skills. *IEEE transactions on Biomedical Engineering*, **48**(5): 579–591.

Rosen, J. et al. (1999). Force controlled and teleoperated endoscopic grasper for minimally invasive surgery – experimental performance evaluation. *IEEE Transactions on Biomedical Engineering*, **46**(10): 1212–1221.

Schostek, S. et al. (2006). Artificial tactile sensing in minimally invasive surgery – a new technical approach. *Minimally Invasive Therapy and Allied Technologies*, **15**(5): 296–304.

Seraji, H., Long, M. K. and Lee, T. S. (1993). Motion control of 7-DOF arms: the configuration control approach. *IEEE Transactions on Robotics and Automation*, **9**(2): 125–139.

Shimachi, S., Fujiwara, Y. and Hakozaki, Y. (2004). New sensing method of force acting on instrument for laparoscopic robot surgery. *Proceedings of the International Conference on Computer Assisted Radiology and Surgery (CARS)*, International Congress Series Vol. 1268, Chicago, IL, pp. 775–780.

Singh, H., Sedaghati, R. and Dargahi, J. (2003). Experimental and finite element analysis of an endoscopic tooth-like tactile sensor. *Sensors*, **1**: 259–264.

Singh, P. et al. (2007). EUS for detection of the hepatocellular carcinoma: results of a prospective study. *Gastrointestinal Endoscopy*, **66**(2): 265–273.

Takashima, K. et al. (2005). An endoscopic tactile sensor for low invasive surgery. *Sensors and Actuators A*, **119**: 372–383.

Tavakoli, M., Patel, R. V. and Moallem, M. (2005). Haptic interaction in robot-assisted endoscopic surgery: a sensorized end-effector. *International Journal of Medical Robotics and Computer Assisted Surgery*, **1**(2): 53–63.

Tavakoli, M. et al. (2006a). Multi-sensory force/deformation cues for stiffness characterization in soft-tissue palpation. *Proceedings of the IEEE International Conference of the Engineering in Medicine and Biology Society*, New York, pp. 847–840.

Tavakoli, M. et al. (2006b). Tool/tissue interaction feedback modalities in robot-assisted lump localization. *Proceedings of the IEEE International Conference of the Engineering*

in Medicine and Biology Society, New York, pp. 3854–3857.

Tholey, G., Desai, J. P. and Castellanos, A. E. (2005). Force feedback plays a significant role in minimally invasive surgery: results and analysis. *Annals of Surgery*, **241**(1): 102–109.

Tholey, G. et al. (2004). Design, development, and testing of an automated laparoscopic grasper with 3-D force measurement capability. *Proceedings of the International Conference on Noise and Vibration Engineering (ISMA 2004)*, Cotin, S. and Metaxas, M. (eds), Leuven, Belgium, pp. 38–48.

Trejos, A. L. et al. (2008). Experimental evaluation of robot-assisted tactile sensing for minimally invasive surgery. *Proceedings of the 2nd IEEE RAS/EMBS International Conference on Biomedical Robotics and Biomechatronics (BioRob 2008)*, October 19–22, Scottsdale, AZ, pp. 971–976.

Van Meer, F. et al. (2004). Si-micromachined 2D force sensor for a laparoscopic instrument. *Proceedings of the International Conference on Computer Assisted Radiology and Surgery (CARS)*, International Congress Series, Vol. 1268, Chicago, IL, p. 1334.

Wellman, P. and Howe, R. D. (1997). Modeling probe and tissue interaction for tumor feature extraction. *Proceedings of the 1997 ASME Summer Bioengineering Conference*, Sun River, OR.

Wellman, P. S. and Howe, R. D. (1999). Extracting features from tactile maps. *Proceedings of the 2nd International Conference on Medical Image Computing and Computer-Assisted Intervention*, Cambridge, UK. Berlin, Springer, pp. 1133–1142.